PROJECTION ARTIFACT SUPPRESSION FOR INNER RETINA IN OCT ANGIOGRAPHY

Yihao Liu[1], *Aaron Carass*[1,2], *Member, IEEE, Angeliki Filippatou*[3], *Yufan He*[1], *Sharon D. Solomon*[4], *Shiv Saidha*[3], *Peter A. Calabresi*[3],*and Jerry L. Prince*[1,2], *Fellow, IEEE*

[1]Dept. of Electrical and Computer Engineering, The Johns Hopkins University, Baltimore, MD 21218
[2]Dept. of Computer Science, The Johns Hopkins University, Baltimore, MD 21218
[3]Dept. of Neurology, The Johns Hopkins University School of Medicine, Baltimore, MD 21287
[4]Wilmer Eye Institute, The Johns Hopkins University School of Medicine, Baltimore, MD 21287

ABSTRACT

Optical coherence tomography (OCT) based angiography devices were introduced for research purposes in 2014 and are now appearing in clinical settings. OCT-A, as this is known, exhibits what is referred to as the *shadowgraphic flow projection artifact*, which causes blood vessels to have an elongated appearance in A-scans. Existing approaches for resolving this artifact rely on the flow signal in superficial layers along the same A-scan to remove projection artifacts in deeper layers, essentially treating the problem as a 1D correction. We however, propose to use characteristics of the projection artifacts in 3D. Specifically, we use the tailing effect of the shadowgraphic flow projection artifact to remove the artifacts in the inner retina. We demonstrate that our projection artifact suppression method produces better OCT-A images when compared with a previously reported correction method, both qualitatively and quantitatively.

***Index Terms*—** Projection Artifact, Optical coherence tomography, Optical coherence tomography angiography

1. INTRODUCTION

Optical coherence tomography (OCT) angiography (OCT-A) is a recently developed imaging modality that provides visualization of the 3D blood vessel networks [1–8]. OCT-A compares sequential OCT B-scans taken at precisely the same cross-section in order to detect contrast induced from flowing blood. However, the presence of shadowgraphic flow projection artifacts obstructs the interpretation of vascular networks in deep layers [9–12]. The projection artifact appears as false blood flow that should be avascular. We can visually identify the projection artifact induced by large vessels in OCT-A by two features: in *en face* angiograms it appears as a duplicated vascular pattern in deep retinal layers by vessels from superficial retina (see Figs. 1(a) and (b)); in cross-sectional angiograms it appears as elongated flow signals right beneath an *in situ* flow (tailing effects) (see Figs. 1(c) and (d)). Current projection artifact removal methods focus on suppressing the duplicated vascular pattern in the 2D *en face* angiogram of the outer retina [13, 14]. Zhang *et al.* proposed a 3D method [9], which identifies a voxel as an *in situ* flow voxel if it has higher intensity-normalized decorrelation values than all shallower voxels in the same A-scan. These methods are similar in the sense that each A-scan is processed independently and no information from adjacent A-scans is considered.

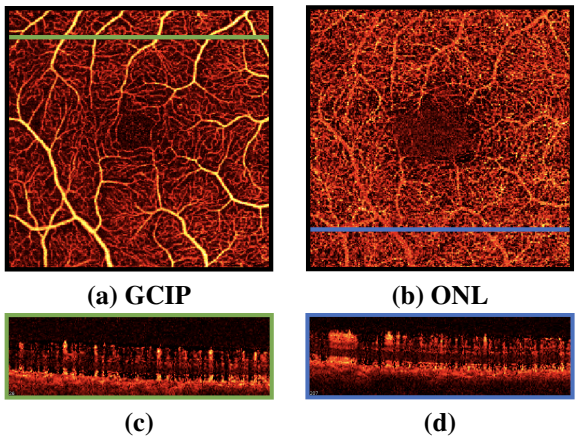

Fig. 1. Shown are the *en face* angiogram produced by maximum projection for the (a) GCIP (GCL and IPL), and the (b) ONL. The cross-sectional angiograms indicated by the green line in (a) and blue line in (b) are shown in (c) and (d). Projection artifact can be identified in (b) by the repeated vascular pattern and in (c) and (d) by elongated flow signal

In this paper, we use the three eigenvalues of the Hessian matrix to detect the tailing effect in 3D OCT-A, and remove them from the inner retina. We demonstrate that our projection artifact suppression method (PAS-OCTA) produce better projection-removed OCT-A compared with the projection-resolved method (PR-OCTA), both visually and numerically.

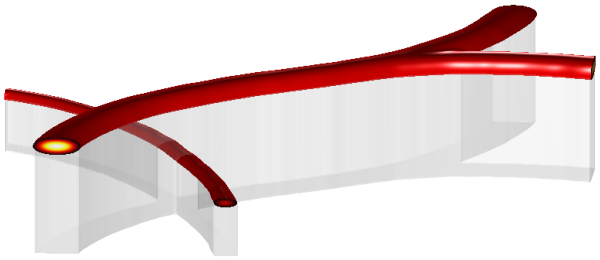

Fig. 2. Demonstration of vessel along with its tailing effects in 3D. The *in situ* flow shows as red vessel and display vesselness while tailing of *in situ* flows (shaded region) shows as a vertical plate-like structure and display plateness. When a capillary intersects with the tailing of a superficial flow, all three eigenvalues at the intersection region are large and show neither plateness nor vesselness.

2. METHOD

The Frangi filter [15] has proved to a successful vessel detector in both 2D and 3D. It uses the eigenvalues ($|\lambda_1| \leq |\lambda_2| \leq |\lambda_3|$) of the Hessian matrix to construct a vesselness measure as

$$\mathcal{V} = (1 - e^{-\mathcal{R}_A^2/2\alpha^2}) e^{-\mathcal{R}_B^2/2\beta^2} (1 - e^{-\mathcal{S}^2/2\gamma^2}), \quad (1)$$

where $\mathcal{R}_A = |\lambda_2|/|\lambda_3|$, $\mathcal{R}_B = |\lambda_1|/\sqrt{|\lambda_2\lambda_3|}$, and $\mathcal{S}$ is the Frobenius norm of the Hessian matrix. It follows the idea that the eigenvalues of the Hessian matrix correspond to the intensity change in three principal direction. For a vessel in 3D, two large eigenvalues and one small eigenvalues are expected and result in a large vesselness in Eqn. 1.

In applying the 3D Frangi filter in OCT-A, we observe that some vessels shown in C-scans have a high vesselness whereas others do not. This observation is explained by the fact that the tailing artifact induced by an *in situ* flow in 3D is shown as a vertical plate-like structure instead of a vessel, as shown in Fig. 2. Two eigenvalues of the Hessian matrix in a plate-like structure are small and one eigenvalue is relative larger. Therefore, we propose to use plateness $\mathcal{P}$ to measure the probability that a structure belongs to a plate:

$$\mathcal{P} = e^{-\mathcal{R}_A^2/2\alpha^2} e^{-\mathcal{R}_B^2/2\beta^2} (1 - e^{-\sqrt[p]{\mathcal{S}}/2\gamma^2}), \quad (2)$$

where $p = 3$ controls the intensity of plate-like structure to be detected. We show in Fig. 3 that the *in situ* flow and its projection artifacts can be identified by plateness while only *in situ* flow are identified by vesselness. Thus, we conclude that projection artifacts in the inner retina can be resolved by suppressing the intensity of voxels with large plateness and small vesselness. We also note that for the situation depicted in Fig. 2, where a capillary in the deeper retina intersects with the projection artifact plate, as it will neither show as a plate-like structure or a vessel-like structure, its intensity is not suppressed. As a result, the integrity of deeper capillary networks can be preserved.

We also observe in the cross-sectional OCT-A in Fig. 3, that contrary to what we expect from the shape of vessels with its projection artifact—a round shape head with tailing—some vessels also have the appearance of spikes above them. This explains why plateness appears both above and below the vesselness in the example shown in Fig. 3.

For an OCT-A and corresponding OCT volume, we resize both to the correct physical dimension, estimated the ILM and IS/OS boundaries by a preprocessing method [16] and approximate the inner retina as the region between those two boundaries. The vesselness $\mathcal{V}$ and plateness $\mathcal{P}$ are calculated in the inner retina for two scales ($\sigma = 1$ and 2 voxels) and then normalized to $[0, 1]$ along each A-scan. To remove false vesselness and plateness created by intensity variation between layers, along each A-scan we keep successive higher vesselness peaks within each plateness peak and remove plateness peaks that contains no vesselness peaks. We define a suppression factor M as:

$$M = \min(1, 1 - \mathcal{V} + \mathcal{P}) \quad (3)$$

The projection artifact is suppressed by multiplying the original OCT-A with the suppression factor M.

Our method does not depend on device-specified normalization, accurate segmentation of layers in the inner retina, or segmentation of vessels in *en face* angiograms. In contrast to the projection-resolve algorithm [9], which removes everything and does not distinguish *in situ* flow, we only remove tailing artifacts that are detected and leave most of the intensity unchanged.

3. RESULTS

3.1. Data

The data used in this work were obtained from a Cirrus angiography prototype spectral-domain OCT system (central wavelength = 840 nm) (Carl Zeiss Meditec Inc, Dublin, CA). 27 OCT-A and corresponding OCT from 19 multiple sclerosis (MS) patients and 8 healthy subjects were used. Each volumetric data set covered a 3 mm by 3 mm scanning area centered at the fovea. Each single B-scan consists of 245 A-scans. For each A-scan, 1024 sampling points were generated along a 2.0 mm axial scan depth.

3.2. Validation

Layers from OCT volume were segmented using AURA tools [16], which segments eight layers (RNFL, GCIP, INL, OPL, ONL, IS, OS, RPE) from the retina. Five layers (RNFL, GCIP, INL, OPL, ONL) in the inner retina were used to calculate the corresponding *en face* angiograms by maximum

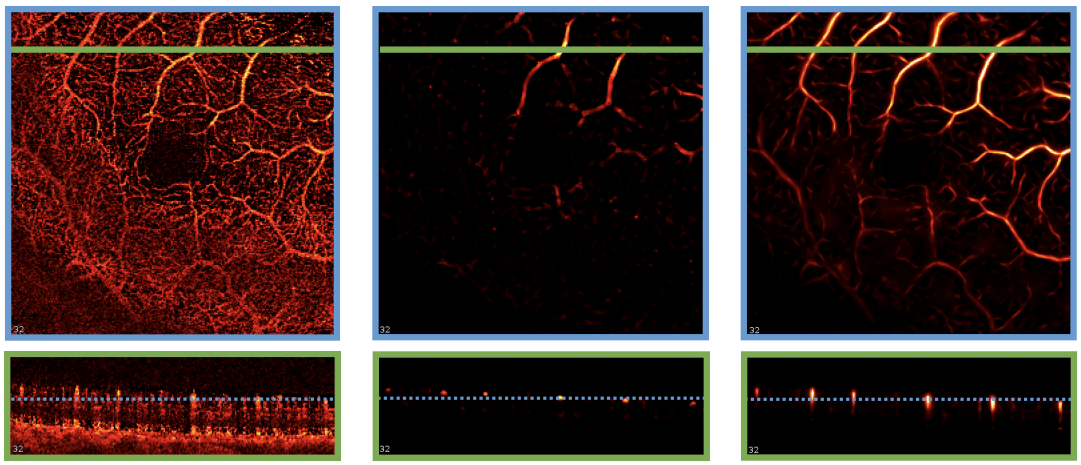

(a) **(b)** **(c)**

Fig. 3. Shown in the top row of **(a)** are an OCT-A C-scan, with the bottom row showing the B-scan corresponding to the green line in the C-scan. Shown in **(b)** and **(c)** are the 3D vesselness and plateness, respectively, for the same regions of the OCT-A image. In the cross-sectiona angiogram, the tailing effect together with the *in situ* flow are identified by plateness whereas vesselness only response to *in situ* flow.

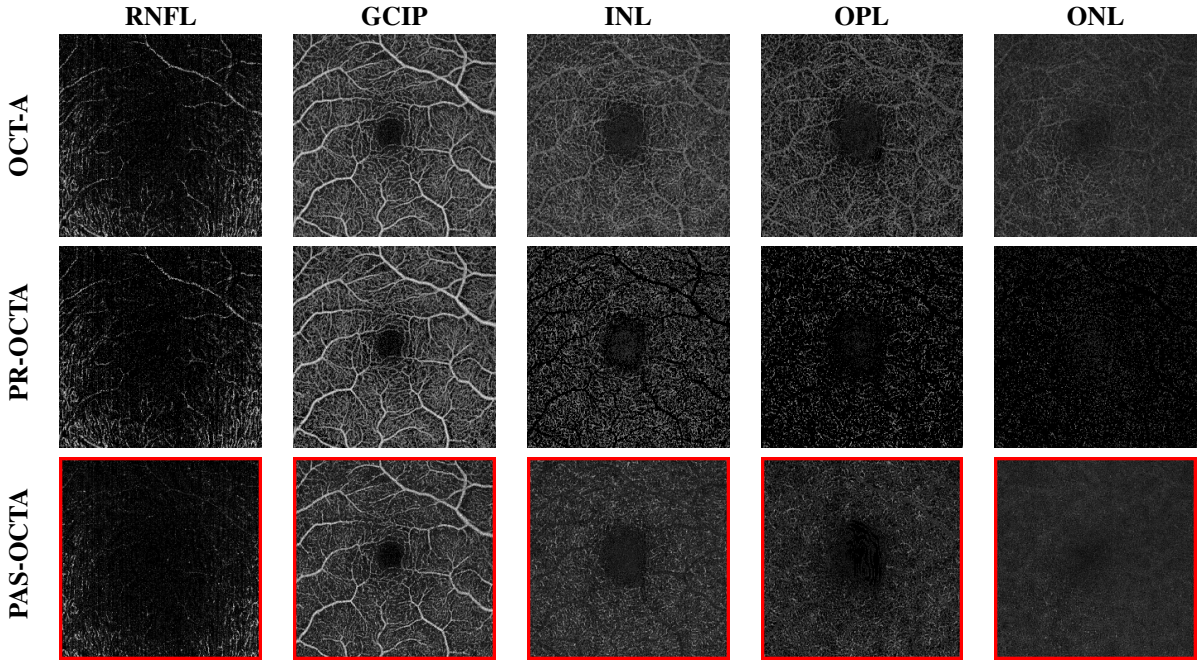

Fig. 4. A comparison of the projection-resolved method (PR-OCTA) and our method (PAS-OCTA) using the *en face* angiograms of 5 layers in the inner retina. The original OCT-A with projection artifacts are shown in the first row. *En face* angiograms from PR-OCTA and PAS-OCTA are shown in the middle row and bottom row, respectively.

projection (Fig. 4). Without projection artifacts, distinct vascular patterns should be visualized in each angiogram and therefore, the Pearson correction coefficient r given by

$$r(X) = \frac{\sum(X - \mu_X)(Y - \mu_Y)}{\sigma_X \sigma_Y} \tag{4}$$

should be close to zero, where X is the *en face* angiogram of a deeper layer and Y is the angiogram of all layers above X. We compared our method to the original OCT-A and to PR-OCTA [9]. All values were adjusted using the correlation coefficient between a 180° rotated OCT-A *en face* angiograms and its unrotated superficial angiogram. It can be seen from

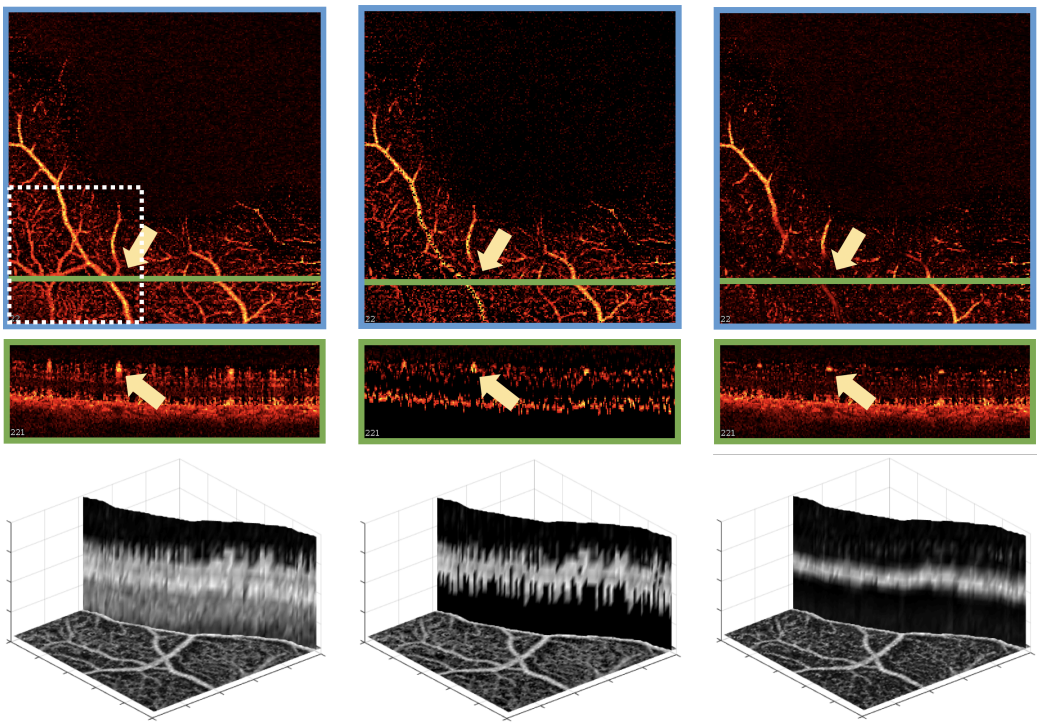

(a) OCT-A **(b) PR-OCTA** **(c) PAS-OCTA**

Fig. 5. A C-scan from OCT-A is shown in (a) top, with the cross sectional angiogram indicated by the green solid line shown in (a) middle. We manually track the locations of a large vessel (indicated by the white arrow in (a) top) in a small region (indicated by the dotted white bounding box in (a) top) and the intensity of those locations along their A-scans are shown in (a) bottom. The corresponding figures produced by PR-OCTA and PAS-OCTA are shown in columns **(b)** and **(c)**, respectively.

Fig. 6 that the absolute value of correlation for our method is smaller across all layers in the inner retina. More importantly, our method does not produce a negative correlation in the OPL and ONL, meaning that for these layers, there are no obvious shadowing effects created by the our algorithm.

Figure 5 illustrate the benefit of detecting projection artifacts in 3D. Even though the *en face* angiograms looks similar for the GCIP layer, if we look at individual C-scans, PR-OCTA produced ill-shaped vessels while PAS-OCTA successfully recovers the round shape vessel.

Our algorithm is implemented in MATLAB and run on a four core 3.1GHz Linux computer. The average computational time for each volume is 72.7 ± 6.0 seconds.

4. CONCLUSION

In this paper, we proposed a 3D shadowgraphic flow projection artifact removal method for the inner retina. The absolute value of correlation coefficients suggests our method produces better results compared with PR-OCTA in terms of removing duplicated vascular pattern in *en face* angiograms of inner retina. We also show that our method is more visually attractive when examined in individual C-scans and in cross-sectional angiograms.

5. ACKNOWLEDGEMENT

This work was supported by the NIH/NEI grant R01-EY024655, NIH/NINDS grant R01-NS082347

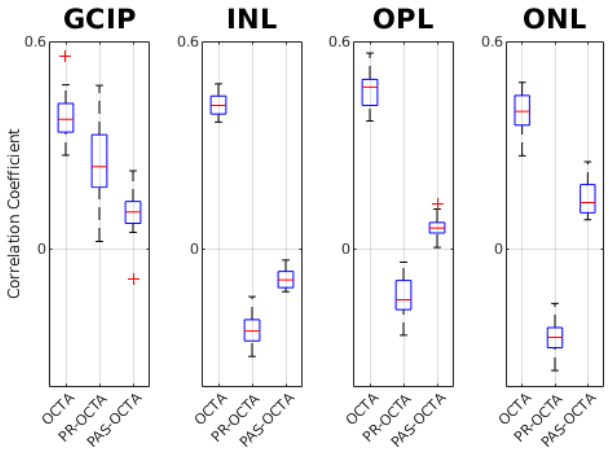

Fig. 6. Correlation between the a deeper layer and and all its superficial layers are calculated for the original OCT-A, PR-OCTA, and our method (PAS-OCTA).

6. REFERENCES

[1] E. Jonathan, J. Enfield, and M. J. Leahy, "Correlation mapping method for generating microcirculation morphology from optical coherence tomography (OCT) intensity images," *Journal of biophotonics*, vol. 4, no. 9, pp. 583–587, 2011.

[2] Y. Jia, O. Tan, J. Tokayer, B. Potsaid, Y. Wang, J. J. Liu, M. F. Kraus, H. Subhash, J. G. Fujimoto, J. Hornegger, et al., "Split-spectrum amplitude-decorrelation angiography with optical coherence tomography," *Optics express*, vol. 20, no. 4, pp. 4710–4725, 2012.

[3] A. Mariampillai, B. A. Standish, E. H. Moriyama, M. Khurana, N. R. Munce, M. K. K. Leung, J. Jiang, A. Cable, B. C. Wilson, I. A. Vitkin, et al., "Speckle variance detection of microvasculature using swept-source optical coherence tomography," *Optics letters*, vol. 33, no. 13, pp. 1530–1532, 2008.

[4] J. K. Barton and S. Stromski, "Flow measurement without phase information in optical coherence tomography images," *Optics Express*, vol. 13, no. 14, pp. 5234–5239, 2005.

[5] J. Fingler, D. Schwartz, C. Yang, and S. E. Fraser, "Mobility and transverse flow visualization using phase variance contrast with spectral domain optical coherence tomography," *Optics Express*, vol. 15, no. 20, pp. 12636–12653, 2007.

[6] J. Fingler, R. J. Zawadzki, J. S. Werner, D. Schwartz, and S. E. Fraser, "Volumetric microvascular imaging of human retina using optical coherence tomography with a novel motion contrast technique," *Optics Express*, vol. 17, no. 24, pp. 22190–22200, 2009.

[7] L. An, J. Qin, and R. K Wang, "Ultrahigh sensitive optical microangiography for in vivo imaging of microcirculations within human skin tissue beds," *Optics Express*, vol. 18, no. 8, pp. 8220–8228, 2010.

[8] R. K. Wang, L. An, P. Francis, and D. J. Wilson, "Depth-resolved imaging of capillary networks in retina and choroid using ultrahigh sensitive optical microangiography," *Optics Letters*, vol. 35, no. 9, pp. 1467–1469, 2010.

[9] M. Zhang, T. S. Hwang, J. P. Campbell, S. T. Bailey, D. J. Wilson, D. Huang, and Y. Jia, "Projection-resolved optical coherence tomographic angiography," *Biomedical Optics Express*, vol. 7, no. 3, pp. 816–828, 2016.

[10] D. Huang, Y. Jia, and S. S. Gao, "Principles of optical coherence tomography angiography," *OCT Angiography Atlas. New Delhi, India: Jaypee Brothers Medical Publishers*, pp. 3–7, 2015.

[11] R. F. Spaide, J. G. Fujimoto, and N. K. Waheed, "Image artifacts in optical coherence angiography," *Retina (Philadelphia, Pa.)*, vol. 35, no. 11, pp. 2163, 2015.

[12] J. P. Campbell, M. Zhang, T. S. Hwang, S. T. Bailey, D. J. Wilson, Y. Jia, and D. Huang, "Detailed vascular anatomy of the human retina by projection-resolved optical coherence tomography angiography," *Scientific reports*, vol. 7, pp. 42201, 2017.

[13] L. Liu, S. S. Gao, S. T. Bailey, D. Huang, D. Li, and Y. Jia, "Automated choroidal neovascularization detection algorithm for optical coherence tomography angiography," *Biomedical Optics Express*, vol. 6, no. 9, pp. 3564–3576, 2015.

[14] A. Zhang, Q. Zhang, and R. K. Wang, "Minimizing projection artifacts for accurate presentation of choroidal neovascularization in oct micro-angiography," *Biomedical Optics Express*, vol. 6, no. 10, pp. 4130–4143, 2015.

[15] A. F. Frangi, W. J. Niessen, K. L. Vincken, and M. A. Viergever, "Multiscale vessel enhancement filtering," in *International Conference on Medical Image Computing and Computer-Assisted Intervention*. Springer, Berlin, Heidelberg, 1998, pp. 130–137.

[16] A. Lang, A. Carass, M. Hauser, E. S. Sotirchos, P. A. Calabresi, H. S. Ying, and J. L. Prince, "Retinal layer segmentation of macular oct images using boundary classification," *Biomedical Optics Express*, vol. 4, no. 7, pp. 1133–1152, 2013.